ADVANCED NANOBIOMED RESEARCH Open Access
www.advnanobiomedres.com

# Reshaping the Inflammatory Environment in Rheumatoid Arthritis Joints by Targeting Delivery of Berberine with Platelet-Derived Extracellular Vesicles

*Qingle Ma, Jinyu Bai, Jialu Xu, Huaxing Dai, Qin Fan, Ziying Fei, Jiacheng Chu, Chenlu Yao, Haoliang Shi, Xiaozhong Zhou,* Lin Bo,* and Chao Wang**

**Rheumatoid arthritis (RA) is a systemic autoimmune disease characterized by inflammation and joint destruction. Herein, an inflamed joint-targeting delivery platform is developed based on platelet-derived extracellular vesicles (PEVs) that are naturally occurring nanoparticles released by platelets, loaded with berberine (BBR) for suppressing the progress of RA. It is found that PEVs could selectively target the inflamed arthritis site in RA mice. In addition, BBR-loaded PEVs exert anti-inflammatory effects by reshaping the inflammatory environment in affected joints. It is shown that intravenous injection of BBR-loaded PEVs into RA mice can effectively reduce joint swelling and bone erosion and restore mobility compared with free drug therapy. This strategy can effectively enhance the efficacy of RA treatment with limited side effects.**

## 1. Introduction

Rheumatoid arthritis (RA) is a chronic inflammatory autoimmune disease, which can lead to disability of joint system, associated with inflammation, swelling, and pain.[1–3] Recent studies suggest that activated inflammatory immune cells including T cells, DCs and macrophages that infiltrate into the joint synovium are responsible for the destruction of joint and cartilage.[4,5] Current agents (e.g., glucocorticoids and nonsteroidal anti-inflammatory agents) have been widely used in clinical applications for RA treatment.[6,7] However, the response to these therapies is very low, depending on the treatment history, especially the course of disease. In addition, strong side effects like teratogenicity, hepatotoxicity, and a high risk of infection limit the use of these agents with a high-frequent dose.[8,9] Therefore, new strategy that targets the affected tissues to enhance the efficacy of RA treatment is urgently awaited.

Recently, cellular delivery systems have become a promising platform for therapeutics delivery.[10–14] Compared with traditional carriers, cell is an inherent component of the body with excellent biocompatibility. At the same time, different types of cells have their unique biological functions, such as chemotaxis, homing properties, immune regulation, and therapeutic effects, etc., which can be utilized to facilitate drug delivery.[15–17] We have previously found that platelet-derived extracellular vesicles (PEVs) which are naturally occurring nanoparticles released by platelets, can selectively target different sites of various inflammation, which is a kind of universal tool for inflammation diagnosis and treatment.[18,19]

Berberine (BBR) is an alkaloid widely studied for the treatment of RA due to their anti-inflammation effect.[20,21] In preclinical studies, BBR has been proven by inhibiting inflammatory proliferation of macrophages and suppressing dendritic cells activation to inhibit inflammation of synovial joints, and by participating in a variety of inflammatory signaling cascades and apoptosis-mediated pathway to ameliorate RA.[22] Here, by loading BBR into PEVs, we showed that berberine-PEVs (BBR-PEVs) could inhibit inflammation by regulating the phenotype of macrophages and dendritic cells. In RA mouse model, high accumulation of BBR-PEVs in affected joints was observed following intravenously administration. Moreover, we found that the mobility of arthritis mice has significantly improved after BBR-PEVs treatment, and the infiltration of inflammatory cells at the arthritis site significantly reduced compared to the free drug treatment group at the same dose. In short, treatment based on our strategy can effectively enhance the efficacy of RA treatment with limited side effects (**Figure 1**a).

Q. Ma, J. Xu, H. Dai, Q. Fan, Z. Fei, J. Chu, C. Yao, H. Shi, C. Wang
Institute of Functional Nano & Soft Materials (FUNSOM)
Jiangsu Key Laboratory for Carbon-based Functional Materials and Devices
Soochow University
Suzhou, Jiangsu 215123, China
E-mail: cwang@suda.edu.cn

J. Bai, L. Bo
Department of Rheumatology
The Second Affiliated Hospital of Soochow University
Suzhou, Jiangsu 215004, China
E-mail: bolin@suda.edu.cn

J. Bai, X. Zhou
Department of Orthopedics
The Second Affiliated Hospital of Soochow University
Suzhou, Jiangsu 215004, China
E-mail: zhouxz@suda.edu.cn

The ORCID identification number(s) for the author(s) of this article can be found under https://doi.org/10.1002/anbr.202100071.



**DOI: 10.1002/anbr.202100071**

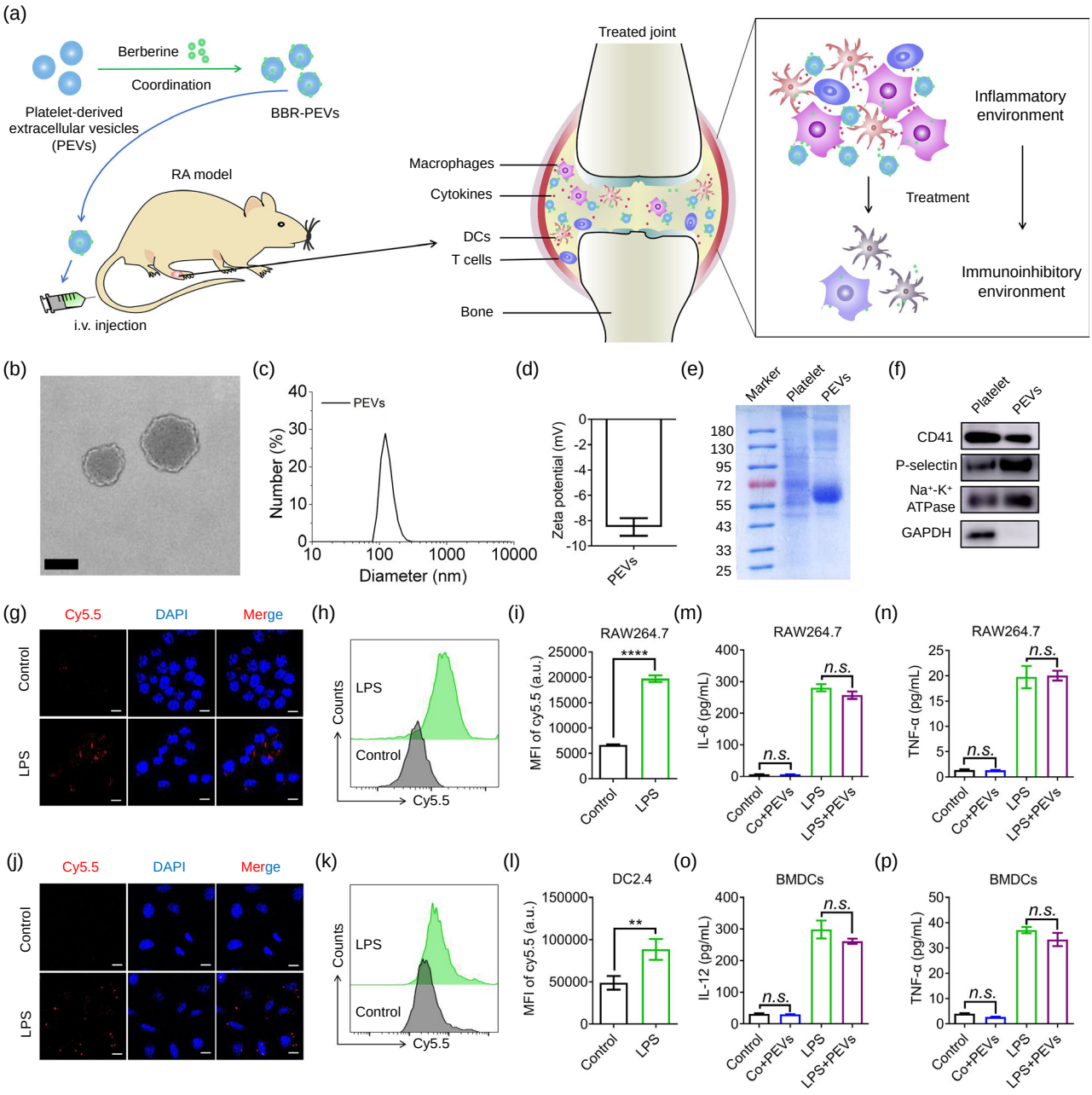


**Figure 1.** Characterization of the platelet-derived extracellular vesicles. a) Schematic illustration of BBR-PEVs to reshape inflammatory environment for treating RA. b) Representative TEM images of PEVs. Scale bars 100 nm. c) Dynamic light scattering data. d) Zeta potential of PEVs in PBS. e) SDS-PAGE of platelet lysate and PEVs with Coomassie brilliant blue staining. f) Western blot results of platelet lysate and PEVs. g) Confocal fluorescence imaging of RAW264.7 macrophages treated with or without LPS followed by treatment of Cy5.5-labeled PEVs. Scale bars 20 μm. h) Representative flow cytometric analysis of untreated and LPS-treated RAW264.7 macrophages adhered Cy5.5-labeled PEVs, and i) corresponding quantification result of mean fluorescent intensity (MFI) of Cy5.5. j) Confocal fluorescence imaging of DC2.4 cells treated with or without LPS followed by treatment of Cy5.5-labeled PEVs. Scale bars 20 μm. k) Representative flow cytometric analysis of untreated and LPS-treated DC2.4 adhered Cy5.5-labeled PEVs, and l) corresponding quantification result of MFI of Cy5.5. m–p) The inflammatory cytokines level in RAW264.7 macrophages and BMDCs culture supernatant of treated with LPS and PEVs. Statistical significance was calculated by one-way ANOVA using the Tukey post-test ($n = 3$–5). *P*-value: $^{**}P < 0.01$; $^{****}P < 0.001$; n.s.; nonsignificant.

## 2. Results and Discussion

### 2.1. Preparation and Characterization of Platelet-Derived Extracellular Vesicles

The preparation of PEVs was based on the protocol previously reported by our laboratory.[18,19] The size and morphology of these vesicles were uniform as revealed by transmission electron microscopy (Figure 1b). The average hydrodynamic size of PEVs was about 140 nm as measured by dynamic light Scattering (DLS) (Figure 1c). The zeta potential of PEVs in phosphate buffered saline (pH = 7.4) exhibited negatively charged (Figure 1d). To confirm whether the vesicles maintained membrane proteins from platelets, sodium dodecyl sulfate (SDS) gel electrophoresis (Figure 1e) and Western blot (Figure 1f, S1, Supporting Information) analysis were then carried out. Cell adhesion-related proteins, such as CD41, P-selectin were detected in the PEVs. In addition, the disappearance of glyceraldehyde-3-phosphate dehydrogenase (GAPDH) (a large number of exists in platelet cytoplasm) in the PEVs indicated the loss of platelet proteins that inside cells.

To study the potential cytotoxicity, PEVs were incubated with three different cell lines, including RAW264.7 macrophages, DC2.4 cells, and human umbilical vein endothelial cells (HUVECs), respectively, for 48 h. CCK-8 assay was used to determine the cell viability, which indicated that PEVs had good biocompatibility (Figure S2, Supporting Information). We further validated the targeting ability of PEVs to inflammatory immune cells including RAW264.7 macrophages and DC2.4 cells in vitro (Figure 1g–l). PEVs labeled with Cy5.5 were cocultured with RAW264.7 macrophages with or W/O lipopolysaccharide (LPS) stimulation. In line with our previous study, we observed an enhanced binding effect of PEVs to LPS-activated RAW264.7 macrophages and DC2.4 cells compared with the untreated cells (Figure 1g–l). We next questioned whether PEVs themselves could induce any activation of RAW264.7 macrophages and bone marrow dendritic cells (BMDCs) cells after coincubation. The phenotype of macrophage was then analyzed by flow cytometry. Macrophages stimulated by LPS showed polarization toward M1-type phenotype, whereas PEVs treatment did not alter their phenotype significantly (Figure S3, Supporting Information). IL-6 and TNF-α were further analyzed in the supernatant 48 h later, which indicated that PEVs did not induce any activation on macrophages significantly (Figure 1m,n). Similarly, we observed similar results in BMDCs (Figure 1o,p). Collectively, these results showed that PEVs effectively bind to the relevant inflammatory cells, while did not aggravate their inflammatory responses significantly.

### 2.2. BBR-PEVs Treatment Effect in Vitro

BBR, an isoquinoline alkaloid which is widely found in herbs such as Rhizoma coptidis and Cypress, has been shown to play an anti-inflammatory and immunosuppressive role in the treatment of arthritis[20,21] (**Figure 2**a). Next, BBR was loaded into the PEVs by hydrophobic interaction as indicated by drug wherein the spectrum of the absorption peak (Figure 2b). Compared with the blank PEVs, the size and zeta potential of the BBR-loaded PEVs (BBR-PEVs) had no significant change (Figure 2c,d). The drug loading percentage was evaluated to be about 6.76% (loaded/added BBR) when the concentration of BBR was 400 $\mu g\,mL^{-1}$ (Figure 2e). Dialysis method (cut off = 10 kD) was used to investigate the release of BBR from the PEVs in vitro. The results implied that BBR-PEVs exhibited a sustained-release profile about 91.9% of drug leaked from the PEVs into the saline within 48 h (Figure 2f).

We next studied the therapeutic effect of BBR-PEVs in vitro. Macrophages play an important role in RA pathophysiology,[23,24] making them as targets for RA treatment. We first studied the immune response of macrophages after BBR-PEVs treatment. As expected, LPS-stimulated macrophages exhibited a typical M1 phenotype. In contrast, BBR or BBR-PEVs treatment remarkably reduced $CD80^+$ levels of LPS-stimulated macrophages, suggesting that BBR-PEVs inhibited LPS-induced inflammatory response and M1 polarization of macrophages (Figure 2g,h). Moreover, BBR-PEVs treatment promoted macrophages to polarize toward M2 phenotype as shown by the increased CD206 expression which was represented as an anti-inflammatory marker (Figure 2i,j). Apart from macrophages, DCs also drive pathological response, leading to chronic proliferative synovitis and joint destruction in RA.[25] After BBR and BBR-PEVs treatment, the expression levels of $CD80^+$ $CD86^+$ and MHC $II^+$/$CD40^+$ on viable $CD11c^+$ cells were significantly decreased (Figure 2k–m) and significant apoptosis of BMDCs was induced as well (Figure 2n), indicating that BBR-PEVs could inhibit the activation of BMDCs. Of note, blank PEVs seemed only to play a role as drug carrier without any influence to the BMDCs. Meanwhile, BBR-PEVs treatment could reduce the production of IL-1β and IL-6 in RAW264.7 macrophages and BMDCs (Figure 2o–r).

### 2.3. In Vivo Behaviors of PEVs

In our previous study, we have demonstrated that PEVs exhibit great targeting capacity to various inflammatory site.[18,19] We subsequently investigated the biodistribution of PEVs in mice with RA. The RA model was successfully established according to the literature[26] (Figure S4, Supporting Information). In our experiment, free Cy5.5 or Cy5.5-labeled PEVs were intravenously (i.v.) injected into normal or RA mice. The mice were imaged at the experimentally designed time points using the in vivo near-infrared fluorescence (NIRF) system. As expected, a higher accumulation of Cy5.5-PEVs were observed in the inflamed joints and claws of RA mice compared with those in normal mice, whereas little signal was detected in RA mice treated with the free dye (**Figure 3**a). Moreover, the PEVs retention time was much longer than other controls. The ex vivo NIRF imaging reinforced the high accumulation of PEVs in the RA joints (Figure 3b,c and S5, Supporting Information). In normal mice, the biodistribution of PEVs was only present in the lung, liver, and kidney, but not in the joints. However, in the RA mice, PEVs had a significant accumulation in the affected ankles and paws, suggesting that PEVs has an excellent accumulation ability at the site of joint inflammation. In addition, fluorescence imaging of ankle joints also showed higher concentration of PEVs in swollen joints compared with free Cy5.5 treatment or in normal mice

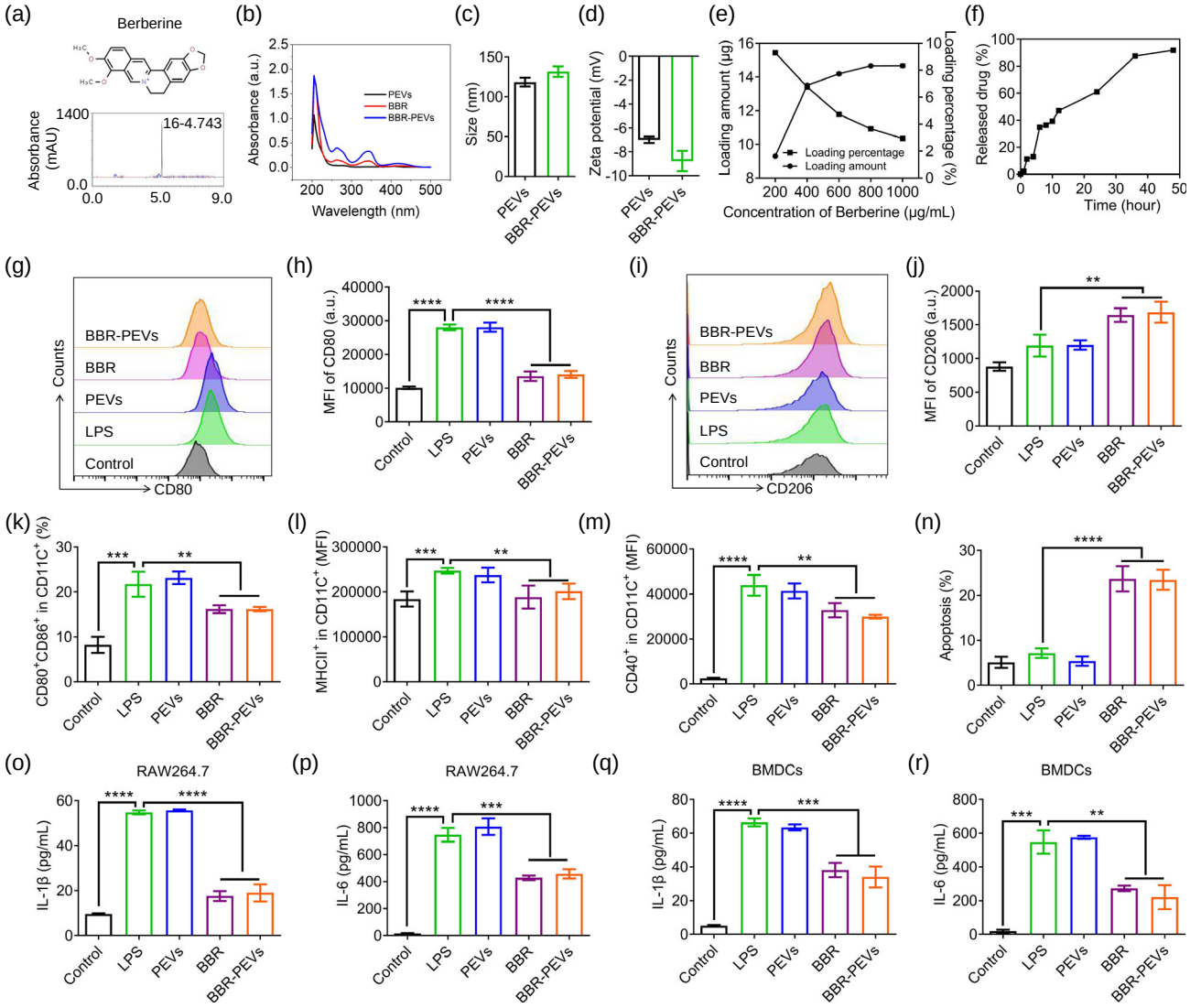


**Figure 2.** BBR-PEVs inhibit activation of macrophages and DCs in vitro. a) Chemical structure and HPLC characteristic peak of BBR. b) Representative UV–vis absorption peaks of PEVs, BBR, BBR-PEVs in the phosphate-buffered saline. c) The size and d) the zeta potential of the PEVs and BBR-loaded PEVs. e) Drug loading amount and efficacy of BBR to the PEVs. f) In vitro release profile of drug-PEVs in the phosphate-buffered saline over 48 h. g) Representative flow cytometric analysis of proinflammatory marker CD80 on RAW264.7 macrophages treated with LPS, PEVs, BBR, and BBR-PEVs, and h) corresponding quantification results of MFI of CD80. i) Representative flow cytometric analysis of anti-inflammatory marker CD206 on RAW264.7 macrophages treated with LPS, PEVs, BBR, and BBR-PEVs, and j) corresponding quantification results of MFI of CD206. k–m) Effect of BBR–PEVs on the expression of CD80, CD86, MHCII, CD40 by BMDCs. n) Analysis of BMDCs apoptosis after various treatments as indicated. o–r) Amount of inflammatory cytokine from o,p) RAW264.7 macrophages and q,r) BMDCs supernatant after various treatments as indicated. Statistical significance was calculated by one-way ANOVA using the Tukey post-test ($n = 3$–5). *P*-value: $^{*}P < 0.05$; $^{**}P < 0.01$; $^{***}P < 0.005$; $^{****}P < 0.001$. Data are means ± SEM.

(Figure 3d). Further, we noted that a higher number of PEVs were captured by $CD45^+$ cells, DCs ($CD45^+$ $CD11C^+$), and macrophages ($CD45^+$ $F4/80^+$) in ankle joints than controls according to the flow analysis (Figure 3e–g), further confirming the targeting ability of PEVs to inflammatory immune cells at RA joints.

To further quantify the targeting ability of PEVs, the radiology imaging technology which has been used in clinic was utilized. In our experiment, PEVs were labeled with $^{125}I$, a radioisotope ion widely used in single-photon emission computed tomography (SPECT) imaging[27,28] (Figure 3h). After the reaction between the $^{125}I$ and PEVs, free $^{125}I$ was removed by multiple washing and centrifugal filtration with phosphate buffered saline (PBS), yielding $^{125}I$-PEVs with a radiolabeling yield of 83%. The obtained $^{125}I$-PEVs exhibited high radioactivity stability in PBS after being placed at 37 °C for 24 h (Figure 3i). Next, we used SPECT imaging to study $^{125}I$-PEVs behavior in vivo. RA mice were injected intravenously $^{125}I$ or $^{125}I$-PEVs (200 μCi) followed

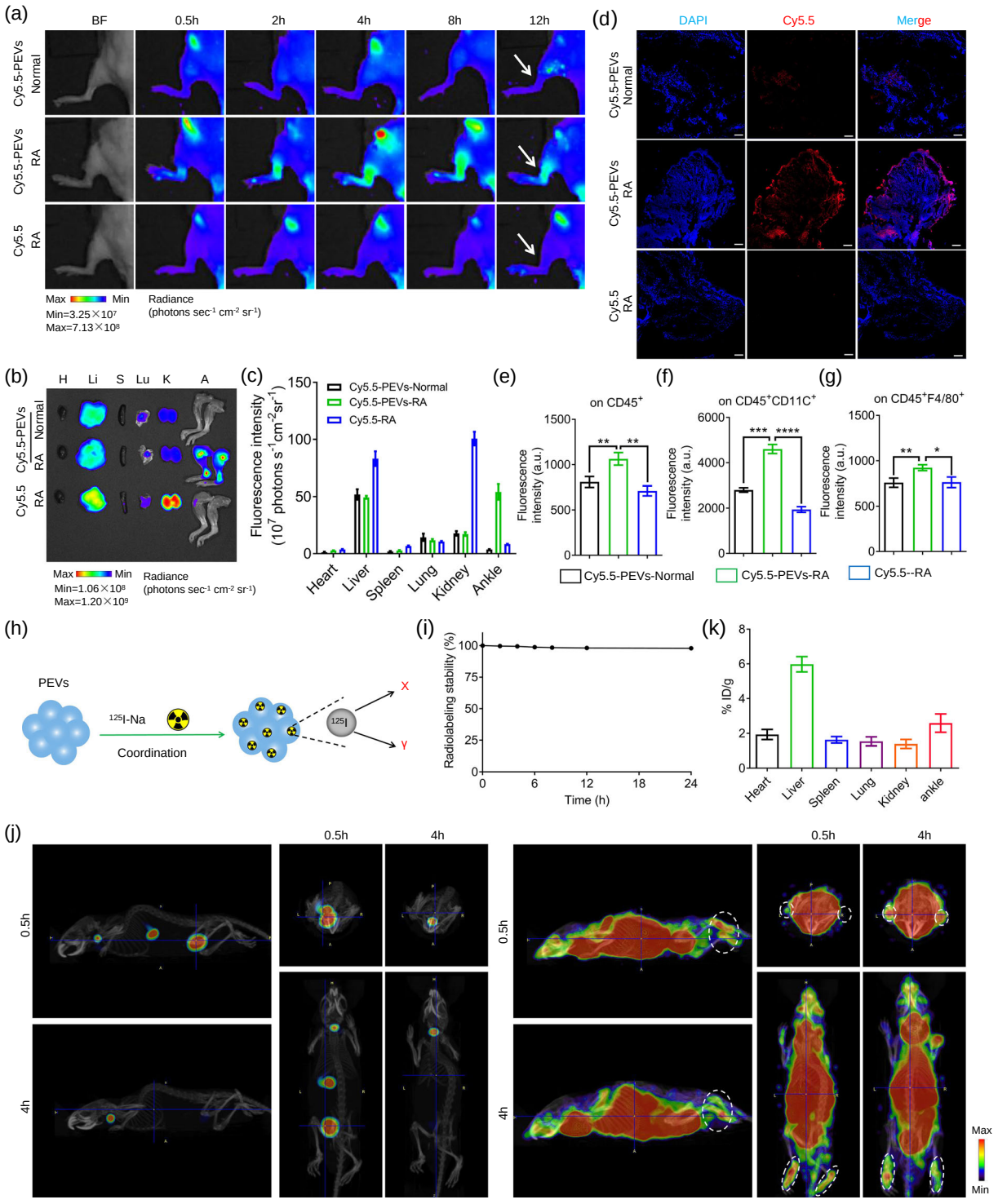


**Figure 3.** Targeting of PEVs toward affected joints. a) In vivo fluorescence imaging of the normal or RA mice after intravenous administration of Cy5.5-labeled PEVs. White arrows: affected joints. b) Ex vivo imaging of major organs after administration of Cy5.5-labeled PEVs after 12 h, and **c**) corresponding quantification result. d) Confocal fluorescence imaging of ankle joint tissue slices of mice after different treatments as indicated, Scale bars 100 μm. e–g) Flow cytometric analysis statistics of fluorescence intensity of Cy5.5 on immune cells. h) Scheme illustrating the $^{125}$I radiolabeling of PEVs for tracing the in vivo fate of nanoparticles. i) Radiolabeling stability of $^{125}$I -labeled PEVs. j) SPECT images of mice at 0.5 and 4 h after intravenous injection of free $^{125}$I (**left**) or $^{125}$I-labeled PEVs (**right**). Joint of mice are highlighted by the dotted circles. k) Biodistribution of $^{125}$I-labeled PEVs measured at 8 h post injection. Statistical significance was calculated by one-way ANOVA using the Tukey post-test ($n = 3$–5). *P*-value: $^{*}P < 0.05$; $^{**}P < 0.01$; $^{***}P < 0.005$; $^{****}P < 0.001$. Data are means ± SEM.

by SPECT imaging at indicated time points (Figure 3j). Obviously, free $^{125}$I mainly occurred in the thyroid gland and excreted through renal metabolism (Figure 3j). The result suggested that the SPECT signal was clearly observed in the joint tissue after intravenous injection with $^{125}$I-PEVs, indicating that PEVs could target at arthritic sites (Figure 3j). Quantification data by gamma counting with major organs demonstrated that the ankle uptake of $^{125}$I-PEVs was determined to be 2.6% ID/g (Figure 3k). Altogether, our data reinforced that PEVs were ideal platforms tending to accumulate at inflamed RA joints.

### 2.4. In Vivo Therapy of BBR–PEVs Infusions

We then evaluated the therapeutic effect of BBR-PEVs on mouse at an established RA disease model. When the paw swelling reached its peak on day 21, the mice received seven intravenous infusions of PBS, PEVs, soluble BBR, or BBR-PEVs over 21 days (**Figure 4**a). During the treatment, the ankle swelling, flexibility of the sole, calculation of clinical scores were recorded daily, respectively. It was observed that the swelling of the hind paws in mice receiving BBR-PEVs was significantly relieved compared with all controls (Figure 4b–e). Beyond day 12, the BBR-PEVs-treated group showed a remarkable ankle swelling suppression effect as compared with BBR-treated mice (Figure 4c). On day 20, the ankle swelling in mice treated with the BBR-PEVs group was reduced by 18.4%, compared with only 9.2% in the BBR-treated group (Figure 4c). In line with ankle swelling, the BBR-PEVs treatment was more effective than the free BBR in both of their sole and peripheral arthritis as determined by the clinical score (Figure 4d,e**)**. In addition, patients with advanced RA often lose their basic mobility. We then evaluated the action of the untreated and treated mice on the rotating cage (Figure 4f, Supporting Information Video). As expected, we observed that the untreated RA mice could barely move. In sharp contrast, the mice treated with the BBR-PEVs had significantly more flexible feet than other control groups, with the highest 13 rotations per minute in the cage (Figure 4g). Taken together, the action studies confirmed the superior therapeutic efficacy of the BBR-PEVs than free drug in treating RA, which has been ascribed to the targeting therapy and higher drug accumulation in affected joints.

The bone tissue morphology was further observed by micro-computed tomography (CT) (Figure 4h–m). Ankle joint inflammation in RA group led to severe bone erosion as shown in the circled area in Figure 4h, and abnormal bone formation in the paws observed in selective erosive arthritis of distal phalanges (Figure 4i). Meanwhile, the bone density was also decreased from 887.3 to 591.9 mg cm$^{-3}$. Treatment with BBR was found to have a nonsignificant improvement with the bone tissue morphology. In contrast, the mice receiving BBR-PEVs exhibited a significantly therapeutic efficiency through the evidence by bone tissue morphology data. The bone mineral density (BMD) of the BBR-PEVs group was increased to 721.6 mg cm$^{-3}$ compared with controls (Figure 4j), suggesting a clear inhibition of bone erosion by the BBR-PEVs treatment. The other parameters, such as trabecular thickness, bone volume/total volume, and bone surface area/bone volume also recovered to those of the normal group after BBR-PEVs treatment (Figure 4k–m**)**. Those results confirmed that the anti-inflammatory effect of BBR-PEVs treatment was better than that of free BBR administration. Moreover, the histological study also showed that, compared with the RA group, synovial and other soft tissues have also been restored (Figure 4n).

Immune cells play a key role in the pathogenesis of RA joint damage and in extra-articular manifestations of the disease. Consequently, we next investigated the alteration of ankle immune cells infiltration after various treatments (**Figure 5**a–f). It was observed that the total percentage of CD45$^{+}$ cells in the ankle joints was significantly reduced in the mice receiving BBR-PEVs compared with those in untreated and the BBR treatment mice (Figure 5a and S6a, Supporting Information). In addition, the population of T cells (CD3), macrophages (CD14, F4/80), and DCs (CD11c) in the ankle joint was further analyzed (Figure 5a–d). Compared with the free drug alone, the abundance of T cells, macrophages, and DCs subsets in mice treated with BBR-PEVs was also found to reduce significantly (Figure 5b–f). Meanwhile, the CD68 and CD80 expression of macrophages and DCs was found downregulated significantly (Figure 5e and S6b,c, Supporting Information). The levels of IL-6 and matrix metalloproteinase (MMP-3) related to the pattern recognition receptor (PRR) signal pathway in the BBR-PEVs group were considerably lower than those in the RA group, which were close to normal group (Figure S6d,e, Supporting Information). The pro-inflammatory cytokines of TNF-α and IL-6 in the tissue homogenate of ankle joints were further tested by enzyme linked immunosorbent assay (ELISA) (Figure 5g,h). The expression of pro-inflammatory cytokines was upregulated remarkably in the RA-untreated group. BBR treatment group did not show an obvious therapeutic effect. On the contrary, the level of these factors was significantly declined in the BBR-PEVs-treated group **(**Figure 5g,h**)**. All these results indicated that the immune microenvironment of inflammatory ankle joints was significantly reshaped by BBR-PEVs therapy.

Next, we evaluated the cytokines level in serum. It is worth noting that the serum levels of various cytokines in the RA model group were significantly increased compared with normal mice, including IL-13, IL-22, IL-17F, IL-9, IL-10, IL-4, IL-6, IL-2, TNF-α, IL-5, and IFN-γ, suggesting that mice with RA-suffered systemic autoimmune inflammatory. Encouragingly, BBR-PEVs administration significantly calmed down all these cytokines level in the serum. All these cytokines were recovered to the normal level after BBR-PEVs treatment compared with the normal mice (Figure 5i, S7, Supporting Information), indicating that systemic inflammation can be relieved by our treatment and simultaneously, better than the free drug efficacy. Next, routine blood parameters, including white blood cells (WBCs), lymphocytes, monocytes, and neutrophils were assessed **(**Figure 5j–l, S8, Supporting Information). These examinations proved that the immune cells in the blood tended to return to normal after treatment with BBR-PEVs. In addition, histochemical staining showed that BBR-PEVs treatment did not induce necrosis or apoptosis of major organs (Figure S9, Supporting Information). Overall, PEVs-based drug delivery system showed an impressive therapeutic efficiency in RA treatment with limited side effect compared with the free drugs.

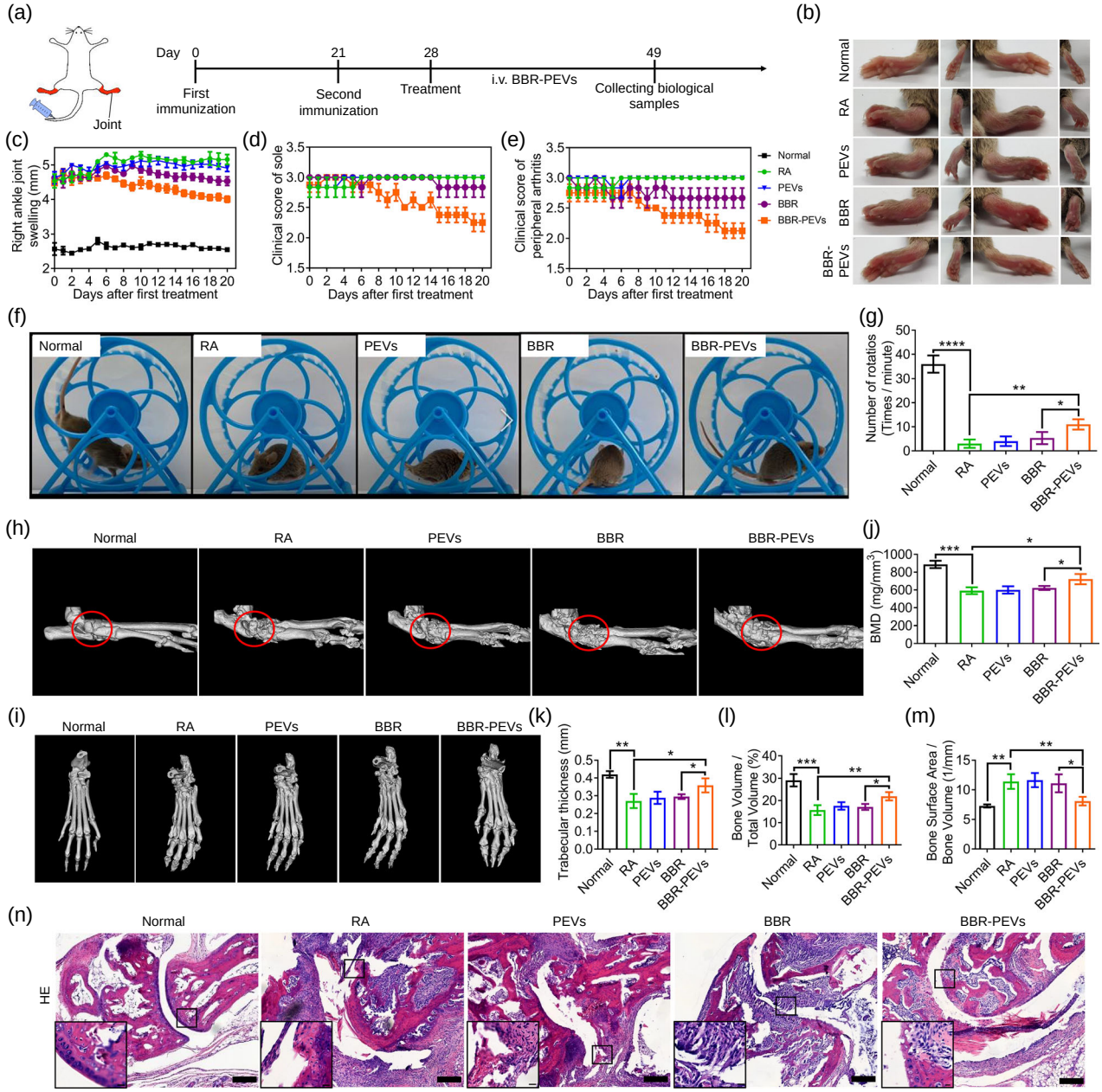


**Figure 4.** In vivo antiarthritis therapy of BBR-PEVs. a) Experimental schedule of the RA model study. After immunization with collagen type II and Freund's adjuvant twice (at day 0 and day 21), the RA model was developed and subsequently received nine intravenous injections of PBS, PEVs, BBR, or BBR–PEVs over 21 days ($n = 5$). Serum was collected 24 h after injection. b) Hind paws of mice at day 49 after first immunization. c–e) Clinical score and swelling of mouse treated in the established stage of RA progression. f) Rotation cage test of RA mouse at day 49 after first immunization (Video was supplied as Supporting Information). g) Rotation per minute of RA mouse at day 49 after first immunization. h,i) Representative micro-CT images of the ankle joints and hind paws. j–m) Analysis of ankle joint bone histomorphometric parameters using micro-CT data. n) Representative HE stained of ankle joints after various treatments as indicated. Scale bars 200 μm. Statistical significance was calculated by one-way ANOVA using the Tukey post-test ($n = 3$–5). *P*-value: $^{*}P < 0.05$; $^{**}P < 0.01$; $^{***}P < 0.005$; $^{****}P < 0.005$. Data are means ± standard error of mean (SEM).

## 3. Conclusions

In summary, we have developed a cellular platform for targeted treatment of RA effectively. Our results indicated that PEVs could target the activated immune cells in vitro and the arthritis site in vivo due to the inherit chemotactic potential. BBR-loaded PEVs effectively inhibited the activation of macrophages and dendritic cells, and showed a strong ability to accumulate at the affected joints to reshape the immune microenvironment and suppress bone erosion and disability. The inflammatory cell infiltration in joints was significantly reduced as compared with free drug treatment. Our strategy provided a new delivery

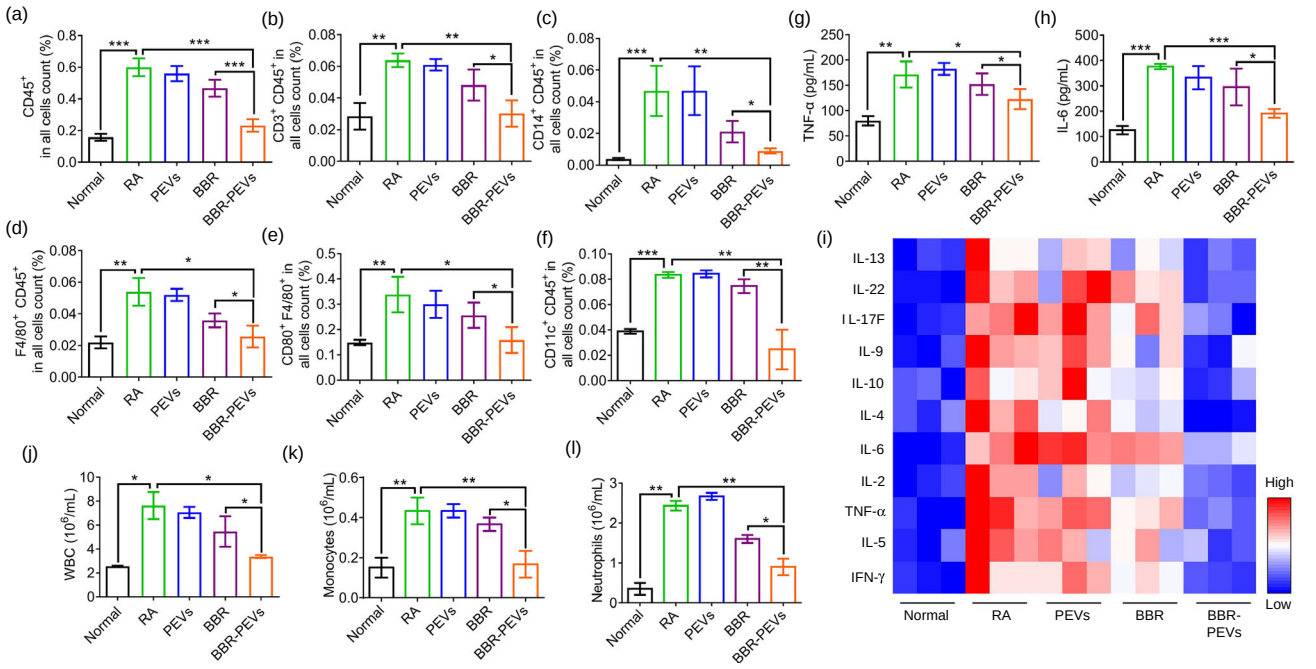


**Figure 5.** Reshaping the inflammatory environment in RA joints by BBR-PEVs. a–f) The proportion of $CD45^+$, $CD3^+$ $CD45^+$, $CD14^+$ $CD45^+$, $F4/80^+$ $CD45^+$, $CD80^+$ $F4/80^+$, and $CD11c^+$ $CD45^+$ in all cells after various treatment. g,h) Inflammatory factors expression of mice ankle joint tissue homogenate after various treatment as indicated. i) The heatmap for showing trends of cytokines level of all individuals in serum. j–l) Blood routine data from mice after various treatment as indicated. Statistical significance was calculated by one-way ANOVA using the Tukey post-test ($n = 3$–5). *P*-value: $^*P < 0.05$; $^{**}P < 0.01$; $^{***}P < 0.005$; $^{****}P < 0.001$. Data are means ± SEM.

platform to target RA-injured tissues and achieve satisfied therapeutic outcomes.

## 4. Experimental Section

*Cell Lines and Mice*: RAW264.7 cells (mouse monocyte macrophages) and DC2.4 cells and HUVECs were originally purchased from American Type Culture Collection (ATCC). DC2.4 cells were maintained in RPMI 1640 medium containing 10% fetal bovine serum (FBS) (Bovogen), 100 U $mL^{-1}$ penicillin (Invitrogen), and 100 U $mL^{-1}$ streptomycin (Invitrogen). Cell line RAW264.7 cells and HUVECs were cultured in Dulbecco's modified Eagle's medium (DMEM) with 10% FBS. BMDCs were isolated from bone marrow cavities of 7–8-week-old C57BL/6 mice according to an established approach[29,30] and then cultured in 1640 medium containing 10% FBS. C57BL/6 mice and DBA/1 mice were purchased from Nanjing Peng Sheng Biological Technology Co., Ltd. Animal experiments were approved by the Laboratory Animal Center and Institutional Review Committee of Soochow University, in compliance with relevant ethical and ethical standards (no. SUDA20200512A01).

*Platelet-Derived Extracellular Vesicles Fabrication*: Platelet-derived extracellular vesicles were collected by natural platelet activation secretion and ultracentrifugation concentration. In detail, fresh blood was collected from the venous plexus of the fundus of healthy C57BL/6 mice, then centrifuged at 100× g for 5 min to extract supernatant platelet-rich plasma (PRP). The pelleted PRP was resuspended in PBS containing prostaglandin E1 (2 μM, Absin) and ethylene diamine tetraacetic acid (EDTA) (5 mM, Sigma-Aldrich) to prevent platelet activation, and platelets were obtained after the centrifugation of PRP at 800× g for 20 min. To extract PEVs, platelet concentrate was activated by thrombin (2 U $mL^{-1}$, Solar bio) in a low-speed shaker at room temperature for 30 min, and was centrifuged at 800× g for 20 min to obtain a supernatant-enriched PEV solution. Then the solution was centrifuged (20 000× g, 40 min) by ultrafiltration tube (3 kD) to further concentrate and collect PEVs. Then Zetasizer-nano-ZS instrument was used to measure the particle size distribution and zeta potential of PEVs in aqueous solution. Transmission electron microscope (TEM) was utilized to observe PEVs morphology. SDS-polyacrylamide gel electrophoresis (SDS-PAGE) and Western Blot were used to detect the protein expression of platelet lysates and platelet-derived extracellular vesicles.

*Cell Adhesion*: Macrophages and DC2.4 cells were inoculated on a 24-well plate with preplated small discs at $1 \times 10^5$ cells/well. After cells were incubated for 12 h, 100 ng $mL^{-1}$ LPS (Biosharp) was added to each well except the control group. Then Cy5.5-labeled PEVs were added to each well and all wells were cultured for another 24 h. After unadhered PEVs were removed with phosphate buffer saline, the adhesion of PEVs was evaluated by flow cytometry and confocal microscope.

*Preparation and Characterization of Drug-Loaded PEVs*: Drugs were first dissolved in dimethyl sulfide (DMSO) and incubated with platelet-derived extracellular vesicles. The size distribution and zeta potential of particles were measured by DLS. In addition, high-performance liquid chromatography (HPLC) was utilized to determine the properties of both drug loading and drug release. The mass fraction of BBR–PEVs was 6.7% when drugs at a concentration of 400 μg $mL^{-1}$.

*Animal Model Induction and Treatment*: DBA/1 mice were injected intradermally with 100 μL bovine type II collagen containing Freund's adjuvant (the volume ratio of the two agents was 1: 1). Three weeks later, bovine type II collagen with the Incomplete Freund's adjuvant 100 μL was injected again. The onset of arthritis occurred on week later, treated with BBR (1 mg $kg^{-1}$) or BBR–PEVs (equal to 1 mg $kg^{-1}$ of BBR) for 3 weeks.

*CCK8 Cytotoxicity Assay*: Hundred microliters of cell suspension was prepared in 96-well plate. The plates were first preincubated for 24 h in an incubator, then different concentrations of substances were added. After incubation for 24 h, 10 μL of CCK8 solution was added to each well,

and plates were incubated for 4 h in an incubator. After incubation, the absorbance of each well at the wavelength of 450 nm was determined by multiwall plate reader.

*Apoptosis Assay*: The treated cells were stained by annexin v-FITC and PI, and apoptosis was detected by flow cytometry. Those annexinv-FITC positive and PI negative cells were apoptotic cells, whereas annexinv-FITC and PI staining double positive were necrotic cells.

*Inflammatory Factor Test*: For the cell supernatant, the cells of each intervention group were incubated for 24 h, and the supernatant inflammatory cytokines were measured by ELISA. For mouse serum, after the blood was statically coagulated, the upper serum was collected by centrifugation and inflammatory factors in serum were evaluated by ELISA.

*Biodistribution of PEVs*: Thirty days after the first immunization of mice, RA mice and normal mice were intravenously injected with Cy5.5-labeled PEVs or free Cy5.5. NIRF imaging was monitored in different groups at different points within 12 h using the IVIS Spectral Imaging System (PerkinElmer Ltd.). Next, all groups of mice were sacrificed and major organs were collected for ex vivo NIRF imaging. In addition, ankle joint tissues were obtained for flow cytometric analysis of the distribution of PEVs on immune cells. Other parts of the ankle joint tissues were analyzed by frozen section and 4′,6-diamidino-2-phenylindole (DAPI) stained the nucleus, followed by observation and analysis of the expression level of Cy5.5 by confocal microscopy.

*Radiolabeling of $^{125}I$*: $Na^{125}I$ Iodogen was first added to the bottom of the reaction tube, then $Na^{125}I$ (Shanghai GMS Pharmaceutical Co., Ltd.) solution and PEVs solution were also added to the tube, which was then shaken gently, and reacted for 30 min at room temperature. At the end of the reaction, the free $Na^{125}I$ and excess reducing agent were removed by centrifugal filtration, and washed with saline until there was no radioactivity in the filtration solution, and the PEVs labeled with radioactive $^{125}I$ was collected.

*SPECT Imaging and in Vivo Distribution of PEVs*: DBA/1 mice were intravenously injected with $^{125}I$-labeled PEVs (200 μCi) and imaging was carried out at 0.5 and 4 h after injection respectively, with SPECT (MILabs, Utrecht, The Netherlands) imaging system. The mice were sacrificed 8 h after injection. All the heart, liver, spleen, lung, kidney, and ankle joints were collected and weighed. Radioactivity in a given mass of tissue was determined.

*Histological Analysis*: After mice were euthanized, tissues and organs were collected and fixed with paraformaldehyde. Tissue sections were embedded in paraffin and stained with hematoxylin&eosin and immunohistochemical staining. The antibodies including CD45, IL-6, MMP-3, CD68, and CD80 were utilized to conduct the analysis. Then images were observed and analyzed under a microscope.

*Flow Cytometry*: According to experimental groups, cell lines or tissues were digested and decomposed into single cell suspension. Those cells were stained with FITC-CD11C, PE-CD86, APC-CD80, PE-MHC II, and PE-CD40 to measure DCs. And other cells stained with PE-CD45, FITC-CD3 to measure T cells, FITC-F4/80, PE-CD80, APC-CD206 were used to analyze the pro-inflammatory and anti-inflammatory phenotypes of macrophages, respectively. After staining, free antibodies were removed by washing, and factors analyzed by flow cytometry.

*Joint Swelling Measurements and Clinical Scores*: From the onset of arthritis until mice were sacrificed, the swelling and clinical scores of the peripheral arthritis were assessed daily. The diameter of the right ankle joint of the mice was measured with a vernier caliper, and the swelling of the mouse joint was evaluated. Each paw had a score ranging from 0 to 3, with 0 representing normal, 0.5 representing swelling of one or more toes, 1 representing mild swelling of the wrist and/or ankle or carpal and/or metatarsal, and 2 representing wrist and/or moderate swelling of the ankle, 3 representing severe swelling throughout the paw and ankle joint.

*Micro-CT Imaging*: To assess the bone injury of mice ankle joints, the ankle joints of mice were fixed in 10% formalin buffer for 1 week and image analysis was carried out. Micro-CT was operated to measure BMD and other morphometric parameters were investigated by experienced blinded researchers.

*Rotational Cage Test Research*: After the last treatment, the exercise capacity of different treated mice was evaluated on a runner device, and the cage then rotates according to the movement of the mice. Normal mice and RA mice were used as experimental controls. All mice underwent simulation training before the rotating cage test to adapt to the experimental environment, and the behavior of mice was recorded by video.

*Statistical Analysis*: All results were expressed as mean ± SEM, as indicated. Analysis of variance was carried out when more than two groups were compared and the results were significant ($P < 0.05$), multiple comparisons. All statistical analyses were carried out using Graph prism (5.0). $^{*}P < 0.05$, $^{**}P < 0.01$, $^{***}P < 0.005$, $^{****}P < 0.005$.

## Supporting Information

Supporting Information is available from the Wiley Online Library or from the author.

## Acknowledgements

This work was supported by National Natural Science Foundation of China (nos. 32022043 and 81802194). This work was also supported by the Program for Jiangsu Specially Appointed Professors to C.W. and the Open Project of Jiangsu Key Laboratory for Carbon–Based Functional Materials & Devices (KJS1905). This work was partly supported by Collaborative Innovation Center of Suzhou Nano Science & Technology, the Priority Academic Program Development of Jiangsu Higher Education Institutions (PAPD), the 111 Project. This work was supported by Postgraduate Research & Practice Innovation Program of Jiangsu Province (KYCX21_2948).

## Conflict of Interest

The authors declare no conflict of interest.

## Author Contributions

C.W. and Q.M. designed the project. Q.M. and J.B. conducted the experiments and collected the data. All authors analyzed and interpreted the data, contributed to the writing of the manuscript, discussed the results and implications, and edited the manuscript at all stages.

## Data Availability Statement

Research data are not shared.

## Keywords

immunosuppressive, platelet-derived extracellular vesicles, rheumatoid arthritis, targeted drug deliveries

Received: May 27, 2021
Revised: June 16, 2021
Published online:

[1] I. B. McInnes, G. Schett, *Lancet* **2017**, *389*, 2328.
[2] J. S. Smolen, D. Aletaha, I. B. McInnes, *Lancet* **2016**, *388*, 2023.
[3] L. An, Z. Li, L. Shi, L. Wang, Y. Wang, L. Jin, X. Shuai, J. Li, *Nano Lett.* **2020**, *20*, 7728.
[4] L. Nerurkar, S. Siebert, I. B. McInnes, J. Cavanagh, *Lancet Psychiatry* **2019**, *6*, 164.
[5] Z. Chen, A. Bozec, A. Ramming, G. Schett, *Nat. Rev. Rheumatol.* **2019**, *15*, 9.

[6] J. F. Ferreira, A. A. A. Mohamed, P. Emery, *Clinics* **2016**, *42*, 33.
[7] G. R. Burmester, J. E. Pope, *Lancet* **2017**, *389*, 2338.
[8] J. S. Smolen, D. Aletaha, *Nat. Rev. Rheumatol.* **2015**, *11*, 276.
[9] J. L. Nam, S. Ramiro, C. Gaujoux-Viala, K. Takase, M. Leon-Garcia, P. Emery, L. Gossec, R. Landewe, J. S. Smolen, M. H. Buch, *Ann. Rheumatic Dis.* **2014**, *73*, 516.
[10] Y. Lu, Q. Hu, C. Jiang, Z. Gu, *Curr. Opin. Biotechnol.* **2019**, *58*, 81.
[11] K. W. Witwer, J. Wolfram, *Nat. Rev. Mater.* **2021**, *6*, 103.
[12] J. Xu, Y. Zhang, J. Xu, G. Liu, C. Di, X. Zhao, X. Li, Y. Li, N. Pang, C. Yang, Y. Li, B. Li, Z. Lu, M. Wang, K. Dai, R. Yan, S. Li, G. Nie, *Adv. Mater.* **2020**, *32*, 1905145.
[13] S. Li, Y. Zhang, J. Wang, Y. Zhao, T. Ji, X. Zhao, Y. Ding, X. Zhao, R. Zhao, F. Li, X. Yang, S. Liu, Z. Liu, J. Lai, A. K. Whittaker, G. J. Anderson, J. Wei, G. Nie, *Nat. Biomed. Eng.* **2017**, *1*, 680.
[14] R. Reshke, J. A. Taylor, A. Savard, H. Guo, L. H. Rhym, P. S. Kowalski, M. T. Trung, C. Campbell, W. Little, D. G. Anderson, D. Gibbings, *Nat. Biomed. Eng.* **2020**, *4*, 52.
[15] C. Wang, D. Wen, Z. Gu, *Bioconjugate Chem.* **2017**, *29*, 702.
[16] O. M. Elsharkasy, J. Z. Nordin, D. W. Hagey, O. G. de Jong, R. M. Schiffelers, S. E. L. Andaloussi, P. Vader, *Adv. Drug Delivery Rev.* **2020**, *159*, 332.
[17] J. Xu, C. Wang, *Explor. Med.* **2021**, *2*, 39.
[18] Q. Ma, Q. Fan, J. Xu, J. Bai, X. Han, Z. Dong, X. Zhou, Z. Liu, Z. Gu, C. Wang, *Matter* **2020**, *3*, 287.
[19] Q. Ma, Q. Fan, X. Han, Z. Dong, J. Xu, J. Bai, W. Tao, D. Sun, C. Wang, *J. Controlled Release* **2020**, *329*, 445.
[20] Z. Wang, Z. Chen, S. Yang, Y. Wang, Z. Huang, J. Gao, S. Tu, Z. Rao, *Inflammation* **2014**, *37*, 1789.
[21] X. Wang, X. He, C.-F. Zhang, C.-R. Guo, C.-Z. Wang, C.-S. Yuan, *Biomed. Pharmacother.* **2017**, *89*, 887.
[22] P. Shen, Y. Jiao, L. Miao, J. Chen, A. A. Momtazi-Borojeni, *J. Cell. Mol. Med.* **2020**, *24*, 12234.
[23] I. A. Udalova, A. Mantovani, M. Feldmann, *Nat. Rev. Rheumatol.* **2016**, *12*, 472.
[24] C. M. Weyand, M. Zeisbrich, J. J. Goronzy, *Curr. Opin. Immunol.* **2017**, *46*, 112.
[25] G. M. Bell, A. E. Anderson, J. Diboll, R. Reece, O. Eltherington, R. A. Harry, T. Fouweather, C. MacDonald, T. Chadwick, E. McColl, J. Dunn, A. M. Dickinson, C. M. U. Hilkens, J. D. Isaacs, *Ann. Rheumatic Dis.* **2017**, *76*, 227.
[26] D. E. Trentham, A. S. Townes, A. H. Kang, *J. Exp. Med.* **1977**, *146*, 857.
[27] J. Cao, Y. Wei, Y. Zhang, G. Wang, X. Ji, Z. Zhong, *ACS Appl. Mater. Interfaces* **2019**, *11*, 18953.
[28] J. Pellico, P. J. Gawne, R. T. de Rosales, *Chem. Soc. Rev.* **2021**, *50*, 3355.
[29] Q. Fan, Q. Ma, J. Bai, J. Xu, Z. Fei, Z. Dong, A. Maruyama, K. W. Leong, Z. Liu, C. Wang, *Sci. Adv.* **2020**, *6*, abb4639.
[30] X. Han, S. Shen, Q. Fan, G. Chen, E. Archibong, G. Dotti, Z. Liu, Z. Gu, C. Wang, *Sci. Adv.* **2019**, *5*, aaw6870.